Published in final edited form as:
Dev Cell. 2011 October 18; 21(4): 746–757. doi:10.1016/j.devcel.2011.08.017.

Atxn1 protein family and Cic regulate extracellular matrix remodeling and lung alveolarization

Yoontae Lee[1,6,7,9], **John D. Fryer**[1,6], **Hyojin Kang**[1,6], **Juan Crespo-Barreto**[5], **Aaron B. Bowman**[1,10], **Yan Gao**[1,6], **Juliette J. Kahle**[1,6], **Jeong Soo Hong**[3], **Farrah Kheradmand**[3], **Harry T. Orr**[8], **Milton J. Finegold**[4], and **Huda Y. Zoghbi**[1,2,5,6,7]

[1]Department of Molecular and Human Genetics, Baylor College of Medicine, Houston, TX 77030, USA

[2]Department of Neuroscience, Baylor College of Medicine, Houston, TX 77030, USA

[3]Department of Medicine, Baylor College of Medicine, Houston, TX 77030, USA

[4]Department of Pathology, Baylor College of Medicine, Houston, TX 77030, USA

[5]Interdepartmental Program in Cell and Molecular Biology, Baylor College of Medicine, Houston, TX 77030, USA

[6]Jan and Dan Duncan Neurological Research Institute at Texas Children's Hospital, Houston, TX 77030, USA

[7]Howard Hughes Medical Institute, Baylor College of Medicine, Houston, TX 77030, USA

[8]Institute of Human Genetics, Department of Biochemistry, Biophysics and Molecular Biology, Department of Laboratory Medicine and Pathology, University of Minnesota, Minneapolis, MN 55455, USA

Summary

Although expansion of CAG repeats in *ATAXIN1* (*ATXN1*) causes Spinocerebellar ataxia type 1, the functions of ATXN1 and ATAXIN1-Like (ATXN1L) remain poorly understood. To investigate the function of these proteins, we generated and characterized *Atxn1L*$^{-/-}$ and *Atxn1*$^{-/-}$; *Atxn1L*$^{-/-}$ mice. *Atxn1L*$^{-/-}$ mice have hydrocephalus, omphalocoele and lung alveolarization defects. These phenotypes are more penetrant and severe in *Atxn1*$^{-/-}$; *Atxn1L*$^{-/-}$ mice, suggesting that Atxn1 and Atxn1L are functionally redundant. Upon pursuing the molecular mechanism, we discovered that several *Matrix metalloproteinase (Mmp)* genes are overexpressed and that the transcriptional repressor Capicua (Cic) is destabilized in *Atxn1L*$^{-/-}$ lungs. Consistent with this, *Cic* deficiency causes lung alveolarization defect. Loss of either Atxn1L or Cic derepresses *Etv4*, an activator for *Mmp* genes, thereby mediating Mmp9 overexpression. These findings demonstrate a critical role of ATXN1/ATXN1L-CIC complexes in extracellular matrix (ECM) remodeling during development and their potential roles in pathogenesis of disorders affecting ECM remodeling.

Correspondence should be addressed to H.Y.Z. (hzoghbi@bcm.edu, 713-798-6523, 713-798-8728 (FAX)).
[9]Present address: Department of Life Science, Pohang University of Science and Technology, Pohang, Kyungbuk 790-784, Republic of Korea
[10]Present address: Department of Neurology and Vanderbilt Kennedy Center for Research on Human Development, Vanderbilt University Medical Center, Nashville, TN 37232, USA

Introduction

The abnormal expansion of a CAG-repeat encoding a polyglutamine (polyQ) tract in *ATXN1* causes the neurodegenerative disease Spinocerebellar ataxia type 1 (SCA1) (Orr et al., 1993; Banfi et al., 1994). The resulting mutant ATXN1 protein acquires toxic functions that cause progressive degeneration of the cerebellum, brainstem, and spinocerebellar tracts (Zoghbi and Orr, 1995). Since *ATXN1* was identified as the gene causing SCA1, the majority of studies on ATXN1 have been focused on uncovering the molecular mechanisms underlying the neurotoxicity of the mutant form of the protein. However, the function of wild-type ATXN1 remains unclear. In an effort to understand the *in vivo* function of ATXN1, we previously generated *Atxn1*-null mice (Matilla et al., 1998). These mice display deficits in spatial and motor learning, but are otherwise viable and fertile with no discernable defects in other tissues (Matilla et al., 1998), suggesting that ATXN1 may not be essential for normal development of peripheral tissues.

A mammalian paralog of ATXN1 was identified and named as ATAXIN1-Like (ATXN1L) (also called Brother of ATXN1, BOAT) (Bowman et al., 2007; Mizutani et al., 2005). ATXN1 and ATXN1L share two highly conserved domains, one in the amino terminal region and the other in the carboxyl terminal region termed Ataxin1 and HMG-box protein1 (AXH) domain (Mizutani et al., 2005), respectively. They are expressed ubiquitously and their tissue distributions are very similar (Mizutani et al., 2005), suggesting that they may be functionally redundant.

To date, most of the clues about the potential functions of these two proteins stem from knowledge of their interactors. ATXN1 and ATXN1L share many common binding partners, including Capicua (CIC), Silencing mediator of retinoid and thyroid hormone receptors (SMRT) and Histone deacetylase 3 (HDAC3) (Mizutani et al., 2005; Lam et al., 2006; Lim et al., 2006). Among the interactors, CIC is of particular interest, because so far it is the only binding partner whose protein levels are significantly reduced in *Atxn1*-null mice (Lam et al., 2006). CIC is an HMG box-containing DNA-binding protein that is evolutionarily conserved from *Caenorhabditis elegans* to human (Jiménez et al., 2000), and functions as a transcriptional repressor by preferential binding to TGAATGA/GA sequences in *Drosophila* and mammals (Ajuria et al., 2011; Kawamura-Saito et al., 2006). In *Drosophila*, Cic functions downstream of receptor tyrosine kinase (RTK) pathways including Torso, EGFR, Ras, Raf, and mitogen-associated protein kinases (MAPKs) to mediate specification of intervein areas in the wing, correct development of the head and tail, and dorsoventral patterning (Jiménez et al., 2000; Roch et al., 2002). In mammalian HEK293 and melanoma cells, MAPK signaling results in phosphorylation of CIC and subsequent loss of CIC-mediated transcriptional repression of *PEA3* group genes (Dissanayake et al., 2010).

Cic exists in a large protein complex of about 2MDa in size together with Atxn1 and Atxn1L in mouse cerebellum (Bowman et al., 2007; Lam et al., 2006). Both ATXN1 and ATXN1L bind to CIC, and compete with each other for its binding (Bowman et al., 2007). In cerebella from *Atxn1*-null mice, Cic protein levels are decreased but mRNA levels are not changed, suggesting that Atxn1 stabilizes Cic through protein-protein interactions (Lam et al., 2006). Moreover, both ATXN1 and ATXN1L can enhance the transcriptional repressor activity of CIC *in vitro* (Lam et al., 2006; Crespo-Barreto et al., 2010), suggesting that some endogenous functions of the ATXN1 protein family must occur in cooperation with CIC.

Given that deletion of *Atxn1* in mice yielded subtle learning and memory phenotypes but no insight into the cellular functions of this protein (Matilla et al., 1998), we hypothesized that

ATXN1 and ATXN1L functionally substitute for each other and that we would need double mutant mice to understand the endogenous functions of the ATXN1 protein family. To this end, we generated *Atxn1L*$^{-/-}$ mice and characterized the phenotypes of either *Atxn1L*$^{-/-}$ or *Atxn1*$^{-/-}$; *Atxn1L*$^{-/-}$ mice. We discovered that loss of Atxn1L destabilizes Cic and affects postnatal viability; that Atxn1 and Atxn1L are functionally redundant, as evident by the developmental defects and perinatal lethality of the double null mice; and that the Atxn1 protein family, together with Cic, regulates extracellular matrix (ECM) remodeling during development.

Results

Atxn1L is critical for viability

We generated *Atxn1L* knock-out mice using homologous recombination to target the gene in embryonic stem cells (Figure S1A). This strategy abolished the expression of Atxn1L (Figure S1B). In a mixed 129S6/SvEv and C57BL/6J background, all of the double null mice died before weaning age (P21) (Table 1). Interestingly, about 40% of *Atxn1*$^{+/-}$; *Atxn1L*$^{-/-}$ mice also died before P21, whereas *Atxn1*$^{-/-}$; *Atxn1L*$^{+/-}$ mice were viable at the weaning age, suggesting that *Atxn1L* is more crucial than *Atxn1* for viability (Table 1). When we back-crossed *Atxn1L* mutant mice to an almost pure C57BL/6J background (more than 7 generations), we found that *Atxn1L*$^{-/-}$ mice were smaller than their littermates (Figures 1A and S1C) and that 50% of them died before P21 (Table S1). Moreover, about 31% of the surviving *Atxn1L*$^{-/-}$ animals developed hydrocephalus (Figure 1B). Symptomatic *Atxn1L*$^{-/-}$ mice developed a dome-shaped head, kyphosis, lethargy, and emaciation sometime between one and four weeks after birth (data not shown). In addition, *Atxn1L*$^{+/-}$ animals developed hydrocephalus at a very low frequency (< 1%) (Figure 1B). Deficiency of *Atxn1L* thus results in growth retardation, hydrocephalus, and perinatal lethality on a C57BL/6J background.

Given the perinatal lethality of the *Atxn1*$^{-/-}$; *Atxn1L*$^{-/-}$ mice, we tried to determine if loss of these two proteins causes embryonic lethality. Of the 178 newborn pups from *Atxn1*$^{+/-}$; *Atxn1L*$^{+/-}$ intercrosses, we observed 11 double null pups. This was consistent with the expected Mendelian ratio (one in sixteen), indicating that loss of Atxn1 and Atxn1L does not cause embryonic lethality (Table 1). However, about 73% (8/11) of the double null pups were cyanotic (Figure 1C) and died within three hrs after birth. This early lethality was also found in *Atxn1*$^{+/-}$; *Atxn1L*$^{-/-}$, *Atxn1*$^{-/-}$; *Atxn1L*$^{+/-}$, and even in *Atxn1L*$^{-/-}$ animals, with lower ratios (less than 20%; data not shown).

To investigate the cause of lethality in the double null mice, we analyzed neonates and E18.5 - E19 embryos by anatomical and histological approaches. Given the hydrocephalus in *Atxn1L*$^{-/-}$ mice, we checked brain morphology and found that the third and lateral ventricles were enlarged in 75% (3/4) of the double null mice at birth, whereas 30% (3/10) of *Atxn1*$^{+/-}$; *Atxn1L*$^{-/-}$ and about 11% (1/9) of *Atxn1L*$^{-/-}$ neonates had this symptom (Figure 1D and Table 2). We also observed an omphalocoele (umbilical hernia), a mild type of abdominal wall closure defect, in about 45% of the double null embryos, and to a lesser degree in *Atxn1*$^{+/-}$; *Atxn1L*$^{-/-}$ embryos (Figure 1E and Table 1). It is known that an omphalocoele results in the loss of internal organs, such as gut and liver, because the mother cannibalizes organs protruding into the umbilical ring in the process of removing the placenta after birth (Thumkeo et al., 2005). Anatomical analysis of organogenesis in the newborn pups revealed that about 45% of the double null pups lost the midgut region from the small intestine to the cecum after birth (Figure 1E and Table 1). The frequency of omphalocoeles and gut loss was higher in *Atxn1*$^{+/-}$; *Atxn1L*$^{-/-}$ animals (17%) than in *Atxn1*$^{-/-}$; *Atxn1L*$^{+/-}$ animals (8%), and these defects were sometimes observed in

Atxn1L$^{-/-}$ (4%), but not in *Atxn1*$^{-/-}$ animals (Tables 1 and 2). Collectively, these data suggest that Atxn1L plays a more important role than Atxn1 for viability.

Alveolarization defects in *Atxn1L*$^{-/-}$ mice

Histological analysis of *Atxn1*$^{-/-}$*; Atxn1L*$^{-/-}$ neonates and E17.5-18.5 embryos revealed no abnormalities in most major organs. However, we found that the double null embryos had a lower proportion of empty space, representing saccules or canaliculi, in lung sections in comparison with double heterozygous littermates (Figures S2A and S2B). This finding suggested that lung development may be abnormal in the double null embryos. Mouse lung development proceeds in five distinct stages: primary budding (E9.5-11.5), pseudoglandular (E11.5-16.5), canalicular (E16.5-17.5), saccular (E17.5-P5), and alveolar (P5-P30) stages (Shi et al., 2007; Greenlee et al., 2007). Given that defects in saccular development and septation at embryonic stages eventually lead to alveolarization defects at postnatal stages (Oblander et al., 2005), we assessed lung morphology in WT, *Atxn1*$^{-/-}$, and *Atxn1L*$^{-/-}$ mice at both early (P6) and late (P17-23) alveolar stages. Histological analysis of lungs showed that lung morphology was comparable among the three different genotypes at P6, whereas alveolarization defects causing air space enlargement were apparent in 65% (13/20) of *Atxn1L*$^{-/-}$ mice at late alveolar stage (P17-23) (Figure 2A and Table 2). Neither *Atxn1*$^{-/-}$ (0/13) nor wild-type mice (0/33) displayed defective alveolarization at this timepoint (Figure 2A and Table 2). Furthermore, the alveolarization defect was more severe in *Atxn1*$^{+/-}$*; Atxn1L*$^{-/-}$ mice compared with *Atxn1L*$^{-/-}$ mice, suggesting that Atxn1 partially compensates for loss of Atxn1L function (Figures S2C and S2D). Early perinatal lethality precluded an analysis of lung alveolarization in the double null mice (Table 2). We also assessed epithelial cell formation in lung tissues by hematoxylin and eosin (H&E) staining and immunohistochemistry for lung epithelial cell specific markers (Clara Cell Secretory Protein (CCSP) for Clara cells and Surfactant Protein C (SFTPC) for type II lung epithelial cells) (Liu et al., 2003) and found that the lung epithelia form normally in *Atxn1L*$^{-/-}$ mice at both early and late alveolar stages (Figure S3A).

To elucidate the molecular mechanism mediating the alveolarization defect, we carried out microarray analyses using lung total RNA from WT, *Atxn1*$^{-/-}$ and *Atxn1L*$^{-/-}$ mice at P6, a timepoint prior to the manifestation of alveolarization defects. We found a total of 406 gene expression alterations (328 up-regulated and 78 down-regulated) with a fold change > 1.2 (*P* value < 0.05) in *Atxn1L*$^{-/-}$ lung tissues (Table S2B), whereas only 54 genes (42 up-regulated and 12 down-regulated) were altered in *Atxn1*$^{-/-}$ lungs (Table S2A). Eighteen genes are shared amongst the differentially expressed genes (DEGs) in *Atxn1*$^{-/-}$ and *Atxn1L*$^{-/-}$ lungs, and about 72% of them (13 out of 18) have a higher fold change in *Atxn1L*$^{-/-}$ mice compared to *Atxn1*$^{-/-}$ mice (Table S2C). Overall, these data suggest that the regulation of gene expression relies more on Atxn1L rather than Atxn1 in lungs at P6. To examine whether particular gene classes were enriched amongst the DEGs in *Atxn1L*-null lung tissue, we analyzed the DEGs for gene ontology (GO) terms related to cellular component using DAVID software (Dennis et al., 2003)**.** We found that the GO terms related to cell surface, plasma membrane and extracellular region were significantly highly ranked among the top 10 categories (Table S2D), suggesting that compositions of the external area of cells might be altered in *Atxn1L*$^{-/-}$ lungs. Specifically, we found one set of genes whose expression changes may be directly responsible for the phenotypes of *Atxn1* and *Atxn1L* double mutants. *Matrix metalloproteinase* (*Mmp*) genes, the critical players in ECM remodeling, were up-regulated in lung tissue from *Atxn1L*$^{-/-}$ mice (Table S2B). Either the overexpression of MMP9 in alveolar macrophages, the induction of MMP12 expression in lung epithelial cells or the loss of *Tissue inhibitor of metalloproteinase 3* (*Timp3*) causes air space enlargement in mouse lungs (Foronjy et al., 2008; Qu et al., 2009; Leco et al., 2001), a prominent phenotype in mice lacking *Atxn1L*. It is also noteworthy that alterations

in MMP levels and ECM formation are closely associated with pathogenesis of hydrocephalus and abdominal wall hernias (Wyss-Coray et al., 1995; Zechel et al., 2002; Antoniou et al., 2009; Suzuki et al., 1996), both highly penetrant in *Atxn1L*-null mice. Therefore, we set out to confirm the *Mmp* gene expression changes observed by transcriptional profiling using qRT-PCR. Among eight *Mmp* genes, we found that *Mmp8, Mmp9, Mmp12* and *Mmp13* levels were significantly up-regulated in *Atxn1L*$^{-/-}$ lung tissues obtained from an independent cohort of animals, consistent with the microarray results (Figure 2B and Table S2B). However, also consistent with the microarray results (Table S2A), the levels of most *Mmp* genes, except for *Mmp12* (*P* value = 0.0542), were not significantly changed in *Atxn1*$^{-/-}$ lung tissues, suggesting that increased levels of multiple *Mmp* genes may be related with the alveolarization defect in *Atxn1L*$^{-/-}$ mice (Figure 2B). We confirmed the overexpression of Mmp9 proteins in lung and meningeal tissues from *Atxn1L*$^{-/-}$ mice compared with their WT littermates (Figure 2C).

Given that alveolar macrophages are the major source for secretion of Mmp9 and Mmp12 in lungs (Greenlee et al., 2007), we investigated whether the number of alveolar macrophages is increased in *Atxn1L*$^{-/-}$ mice compared with WT mice. We counted the number of alveolar macrophage cells in bronchoalveolar lavage fluid (BALF) and found that there is no difference in the alveolar macrophage cell numbers between WT and *Atxn1L*$^{-/-}$ mice (Figure S3B), suggesting that up-regulation of a subset of *Mmp* gene levels in *Atxn1L*$^{-/-}$ mice is not simply due to increase in the number of macrophage cells in lungs. Given that TIMPs are physiological inhibitors for MMPs, we checked whether levels of *Timp* genes are changed in *Atxn1L*$^{-/-}$ mice. Microarray and qRT-PCR analyses showed that the levels of *Timp* genes were not significantly changed in lungs from *Atxn1L*$^{-/-}$ mice (Figure 2D and Table S2B).

We further assessed the integrity of ECM formation in *Atxn1L*$^{-/-}$ lung tissues by Verhoeff staining for elastin to investigate whether the overexpression of Mmps indeed affects ECM formation in *Atxn1L*$^{-/-}$ mice. Reduction in the area occupied by elastic fibrils within the alveolar walls was evident in symptomatic 7-9 month old *Atxn1L*$^{-/-}$ mice compared with WT mice (Figures 2E and 2F). These data suggest that loss of Atxn1L causes the alveolarization defects associated with the overexpression of Mmps and the decrease in elastic fiber formation in the lungs.

Loss of Atxn1/Atxn1L-Capicua complexes causes the lung alveolarization defect

To gain further insight into the molecular mechanism underlying the phenotypes and the overexpression of a subset of *Mmp* genes in the mutant animals, we focused on a common interactor of ATXN1 and ATXN1L. Both Atxn1 and Atxn1L bind the transcriptional repressor Cic to form endogenous protein complexes in mouse cerebella (Bowman et al., 2007; Lim et al., 2006). Co-expression of either ATXN1 or ATXN1L with CIC synergistically enhanced the transcriptional repressor activity of CIC *in vitro* (Lam et al., 2006 ; Crespo-Barreto et al., 2010), suggesting that ATXN1/ATXN1L and CIC could cooperatively function to regulate expression of CIC target genes. To investigate whether this functional relationship between ATXN1/ATXN1L and CIC is conserved in other peripheral tissues or restricted only in brain, we checked expression profiles of Atxn1, Atxn1L and Cic in various tissues from E18.5 embryos. We found that their expression patterns were very similar, suggesting that Atxn1/Atxn1L and Cic might function together in peripheral tissues during embryogenesis (Figure 3A). Previous work revealed that loss of Atxn1 reduces levels of Cic protein, without change in *Cic* mRNA levels, in adult mouse cerebella (Lam et al., 2006). Accordingly, we checked Cic levels in brain and lung tissues from E18.5 embryos of five different genotypes. We found that both Atxn1 and Atxn1L are required for maintaining the steady state level of Cic but that Cic levels are more dramatically decreased in *Atxn1*$^{+/-}$*; Atxn1L*$^{-/-}$ than in *Atxn1*$^{-/-}$*; Atxn1L*$^{+/-}$ mice,

suggesting that Atxn1L plays a critical role for stabilizing Cic during embryogenesis (Figures 3B and 3C). The predominant role of Atxn1L for Cic stabilization was also observed in lung tissue during postnatal stages. Reduced levels of Cic protein were more apparent in *Atxn1L*$^{-/-}$ mice compared with *Atxn1*$^{-/-}$ mice at P6 (Figures 3D and 3E), whereas *Cic* mRNA levels were not significantly changed in *Atxn1L*$^{-/-}$ mice (data not shown).

Given the critical roles of Atxn1L in both the phenotypes found in mutant animals and the stabilization of Cic, we hypothesized that the phenotypes might be related to reduced Cic levels. Recently, we generated *Cic* mutant (*Cic-L*$^{-/-}$) mice using ES cells in which the *Cic* gene is targeted by a β-geo genetrap cassette (Baygenomics). The expression of the longer form of Cic (Cic-L) is completely abolished in these mice, whereas about 15% of the short form of Cic (Cic-S) is still expressed in the cerebella (Fryer and Zoghbi, unpublished data). The majority of *Cic-L*$^{-/-}$ mice died before weaning age (P21), and some of the survivors were smaller than their littermates on the C57BL/6J background (Fryer and Zoghbi, unpublished data). To test the hypothesis that Cic deficiency causes alveolarization defects comparable to the defects found in *Atxn1L*-null mice, we examined the lung morphology and Mmp9 levels in the *Cic-L*$^{-/-}$ survivors. The *Cic-L*$^{-/-}$ mice indeed have increased levels of Mmp9 and severe alveolarization defects, compared with *Cic-L*$^{+/-}$ mice (Figures 3F and 3G). These data suggest that the lung alveolarization defect in *Atxn1* and *Atxn1L* double mutant mice are likely due to deficiency of Atxn1/Atxn1L-Cic complexes.

Derepression of *Pea3* group genes in mutant mice

Given the possibility that deficiency of Atxn1/Atxn1L-Cic complexes is responsible for the alveolarization defect, we turned our attention to the Cic target genes that may contribute to the alteration of *Mmp* gene expression in *Atxn1L*$^{-/-}$ mice. Among the significantly up-regulated genes (fold increase >1.2, *P* value <0.05) in *Atxn1L*$^{-/-}$ lung tissues, we searched for CIC binding motifs (TGAATGA/GA) within a 1 kb region upstream from the transcriptional start site. We also considered conservation scores of the 30 vertebrate species from the phastCons track of the UCSC Genome Browser (http://genome.ucsc.edu/) (Siepel et al., 2005). We discovered that four genes, *Etv4* (also known as *Pea3*), *Prkcb*, *Nfkbie*, and *Runx3*, had between one to four CIC binding motifs and were significantly up-regulated by 1.2-1.4 fold (*P* value < 0.01) (Table S2B). Among these genes, *Etv4* got our attention, not only because it has the highest fold increase and significance (Table S2B), but also because it is known as a transcriptional activator for many different types of *MMP* genes (Gum et al., 1996; Yan and Boyd, 2007). Moreover, more than one purine rich PEA3 element (A/CGGAA/T) exists in promoter regions (within 5 kb upstream from the transcription start site) of most mouse *Mmp* genes (Table S3). Etv4 is one of the members in Pea3 group transcription factors, which include Etv1/Er81 and Etv5/Erm. All *Pea3* group members have at least one Cic binding motif in their promoter regions (Figure 4A). Notably, previous studies have also verified that their expression is regulated by CIC (Kawamura-Saito et al., 2006; Dissanayake et al., 2011). To examine the possibility that expression of *Pea3* group genes could be regulated by Cic in lung, we investigated Cic promoter occupancy of *Pea3* group genes in lung by chromatin immunoprecipitation (ChIP) using anti-Cic antibodies followed by PCR of the promoter regions containing Cic binding motifs (Figures 4A and 4B). We found that Cic is indeed bound to the promoters of *Pea3* group genes in lung cells (Figure 4B). Next, we checked the levels of *Pea3* group genes in lung tissues from 6 day-old WT, *Atxn1*$^{-/-}$, and *Atxn1L*$^{-/-}$ mice by qRT-PCR. The levels of *Etv1* and *Etv4* were significantly up-regulated in *Atxn1L*$^{-/-}$ mice, whereas *Atxn1*$^{-/-}$ mice did not have significant alterations in the levels of these three genes (Figure 4C), suggesting that Atxn1L plays a more important role than Atxn1 in regulation of *Pea3* group gene expression and consistent with the predominant effect of Atxn1L deficiency on destabilization of Cic

(Figure 3E). An increase in Etv4 protein levels in *Atxn1L*$^{-/-}$ mice was also confirmed by Western blot analysis (Figure 4D). We then compared the levels of *Pea3* group genes among *Atxn1* and *Atxn1L* double mutants. The levels of *Pea3* group genes were most dramatically and significantly up-regulated in the double null embryos at E18.5 (Figure 4E). Moreover, the levels of *Pea3* group genes were inversely correlated with the levels of Cic proteins, demonstrating that mice with the most significant reduction in Cic levels had the highest fold change in *Pea3* group gene expression (Figures 3C and 4E). These data provide further support to the idea that the loss of Atxn1/Atxn1L leads to derepression of Cic target genes due to destabilization of Cic.

Derepression of *Etv4* increases Mmp9 levels in alveolar macrophages

Previous reports demonstrated that ETV4 activates transcription of *MMP9* in various cancer cell lines (Hida et al., 1997; Qin et al., 2008). Enhanced expression of MMP9 has been observed in alveolar macrophages from chronic obstructive pulmonary disease (COPD) patients (Finlay et al., 1997). Furthermore, transgenic overexpression of MMP9 in alveolar macrophages causes emphysema in mice and is associated with the loss of alveolar elastin (Foronjy et al., 2008). Therefore, we hypothesized that increased levels of Etv4 may lead to the overexpression of Mmp9 in either *Atxn1L*$^{-/-}$ or *Cic-L*$^{-/-}$ mice. To test this hypothesis, we first investigated whether Etv4 regulates expression of Mmp9 in mouse alveolar macrophage cell line (MH-S) by knocking-down *Etv4*. The levels of Mmp9 are reduced upon treatment with two different siRNAs against *Etv4* in MH-S cells, suggesting that Etv4 indeed regulates expression of Mmp9 in alveolar macrophages (Figure 5A). However, knocking-down *ETV4* did not change the levels of *MMP9* in immortalized lung epithelial cells (A549) (Figure S4), suggesting that regulation of MMP9 expression by ETV4 might be cell type-specific. Next, we treated MH-S cells with siRNAs against *Cic* to examine whether knocking-down *Cic* up-regulates the levels of Mmp9 and *Etv4*. Expression of both Mmp9 and *Etv4* is indeed highly induced in the cells treated with *Cic* siRNAs compared with the cells treated with negative control siRNAs (Figures 5B-5D). Finally, we transfected *Etv4* siRNAs in cells with reduced Cic. The addition of *Etv4* siRNAs rescued the levels of both *Etv4* and Mmp9 to almost normal levels without affecting Cic knock-down efficiency, suggesting that loss of Cic mediates overexpression of Mmp9 in alveolar macrophages by derepression of *Etv4* (Figures 5B-5D).

Discussion

In this study, we set out to understand the *in vivo* function of the ATXN1 protein family by generating and characterizing both *Atxn1L*$^{-/-}$ and *Atxn1*$^{-/-}$*; Atxn1L*$^{-/-}$ mutant animals. We uncovered several developmental deficits potentially caused by misregulation of ECM remodeling in the mutant mice. These phenotypes appear to be caused by a deficiency of Atxn1/Atxn1L-Cic complexes because we found that stability of Cic proteins relies on both Atxn1 and Atxn1L and that *Cic-L*$^{-/-}$ mice have the same developmental abnormalities found in the *Atxn1* and *Atxn1L* double mutant animals. As a consequence, loss of Atxn1/Atxn1L-Cic complexes derepresses Cic target genes including *Pea3* group genes, leading to overexpression of Mmps and defects in ECM remodeling.

Functional redundancy and differences between ATXN1 and ATXN1L

Given that ATXN1 and ATXN1L share conserved domains and several interactors and that their expression profiles are very similar (Mizutani et al., 2005), we hypothesized that functional redundancy of Atxn1L might compensate for the deficiency of Atxn1 function in *Atxn1*-null mice. Loss of both Atxn1 and Atxn1L results in early perinatal lethality and several developmental abnormalities during embryogenesis. Moreover, a complete removal of *Atxn1* from *Atxn1L*-null mice augments the incidence and severity of the phenotypes in

Atxn1L-null mice, suggesting that Atxn1 partially compensates for the loss of Atxn1L function. Interestingly, our data consistently show that Atxn1L is more critical than Atxn1 in the manifestation of all the phenotypes. This phenomenon seems to be closely associated with the dominant role of Atxn1L in stabilization of Cic and raises the question of how this occurs. One simple explanation is that the absolute number of ATXN1L molecules might be much greater than that of ATXN1 such that ATXN1L-CIC complexes predominate in most cells. Another explanation is that CIC may prefer ATXN1L, rather than ATXN1, as a binding partner. In this case, it would be important to do an in-depth comparative structural analysis between ATXN1 and ATXN1L, especially for the AXH domain that is responsible for the interaction of ATXN1 with CIC (Lam et al., 2006). Overall, the data in this study show that Atxn1 and Atxn1L are functionally redundant and that Atxn1L plays a pivotal role in development.

ATXN1 protein family regulates ECM remodeling *in vivo*

Our data showed that loss of Atxn1L causes the lung alveolarization defect associated with overexpression of *Mmp* genes and reduction in elastic fibril formation within alveolar walls. Many genetic studies of mice that are defective in regulation of ECM remodeling have pointed to the pivotal role of the ECM remodeling in lung alveolarization. Transgenic overexpression of either MMP1 or MMP9 in lungs leads to progressive adult-onset (at around 4-6 months after birth) emphysema, whereas mice lacking *Timp3* spontaneously develop enlarged air spaces in the lung at 2 weeks after birth, with disease severity progressing with age (Foronjy et al., 2003; Foronjy et al., 2008; Leco et al., 2001). These studies not only suggest that a tight regulation of Mmp activity is critical for normal lung development, but also indicate that hyperactivation of multiple Mmp enzymes causes an earlier onset of lung alveolarization defects rather than the overexpression of a single *MMP* gene. We found that *Atxn1L*-null mice have increased levels for *Mmp* genes (*Mmp8, Mmp9, Mmp12* and *Mmp13*) in the lung at P6 and develop the alveolarization defect leading to enlarged air spaces at late alveolar stages (P17-P23). Comparing our findings with the previous reports, increased levels of *Mmp8, Mmp9, Mmp12* and *Mmp13* might cooperatively contribute to the onset of lung alveolarization defects in *Atxn1L*$^{-/-}$ mice. It is interesting that the *Atxn1* and *Atxn1L* double mutant mice have other phenotypes, which are also reminiscent of defects in ECM formation. Hydrocephalus is caused by obstruction in circulation of cerebrospinal fluid (CSF) leading to accumulation of CSF and expansion of ventricles in brain. The ECM composition in the meninges, where the arachnoid villi are located, is regarded as an important environment for absorption of CSF into arachnoid villi (Zhao et al., 2010). Several studies using genetically engineered mouse models have indicated that alterations in Mmp9 levels are associated with development of hydrocephalus (Zechel et al., 2002; Muñoz et al., 2006; Oshima et al., 1996). Therefore, our finding that Mmp9 levels are up-regulated in the meninges from *Atxn1L*$^{-/-}$ mice may explain the onset of hydrocephalus in *Atxn1L*$^{-/-}$ mice. Abdominal wall hernias are considered a disease of the ECM because disturbances in collagen metabolism are strongly associated with these developmental defects in humans (Antoniou et al., 2009). Several clinical studies have shown that *MMP1*, *MMP2*, *MMP9* and *MMP13* are overexpressed in patients with abdominal wall hernias (Antoniou et al., 2009). In this regard, the omphalocoele in *Atxn1*$^{-/-}$*; Atxn1L*$^{-/-}$ double mutant embryos might result from the role of Atxn1 protein family in ECM formation. Taken together, our findings suggest that the ATXN1 protein family plays a critical role in ECM remodeling during development.

ATXN1/ATXN1L-CIC complexes are critical for the molecular pathway regulating ECM remodeling

In this study, we found that Cic levels are decreased whereas *Pea3* group genes are overexpressed in *Atxn1*$^{-/-}$*; Atxn1L*$^{-/-}$ double mutant animals. We also verified that

expression of *Pea3* group genes is regulated by Atxn1/Atxn1L-Cic transcriptional repressor complexes in lung cells. Given that more than one purine rich PEA3 element (A/CGGAA/T) exists in promoter regions of most *Mmp* genes, overexpression of a subset of *Mmp* genes in *Atxn1L*$^{-/-}$ mice may be mediated by derepression of *Pea3* group genes. Indeed, we showed that derepression of *Etv4* due to knock-down of *Cic* mediates the overexpression of Mmp9 in the alveolar macrophage cells. It has also been shown that Etv4 regulates *Mmp13* expression in hepatic stellate cells (Díaz-Sanjuán et al., 2009). Altogether, our study demonstrates that ATXN1/ATXN1L-CIC complexes directly regulate the expression of *PEA3* group genes, thereby mediating the regulation of a subset of *MMP* genes.

Potential roles of ATXN1/ATXN1L-CIC complexes in the pathogenesis of disorders involving ECM remodeling

The pathogenesis of many human diseases, such as rheumatoid arthritis, asthma, artherosclerosis, hypertension and fibrosis, is strongly associated with the misregulation of ECM remodeling due to alterations in MMP levels. Moreover, in cancer, altered proteolysis leads to unregulated tumor growth, inflammation, tissue invasion and metastasis (Kessenbrock et al., 2010). Indeed, it is well known that increased expression of MMPs is associated with cancer cell invasion and migration (Roy et al., 2009). Additionally, overexpression of *PEA3* group genes have been found in many different human tumors including breast cancer, nonsmall cell lung carcinoma and leukemia (Kurpios et al., 2003). Given the critical roles of MMPs and PEA3 group proteins in tumorigenesis and cancer metastasis, our data suggest that the ATXN1/ATXN1L-CIC complex might potentially affect tumorigenesis or cancer metastasis. Intriguingly, one frameshift and three missense mutations in the *CIC* gene have been identified in patients with breast cancer and lung cancer cells (Sjöblom et al., 2006; Kan et al., 2010). Recently, mutations in *CIC* gene were found in tumor tissue from patients with oligodendrogliomas (OD), the second most common malignant brain tumor in adults (Bettegowda et al., 2011). Moreover, analysis on the expression profiles of *ATXN1*, *ATXN1L* and *CIC* in various cancer samples using the Oncomine database analysis tool (http://www.oncomine.org/) reveals that the levels of all three genes are significantly down-regulated in breast and brain cancer patients (data not shown), suggesting that loss of ATXN1/ATXN1L-CIC functions might contribute to tumorigenesis of particular types of cancer. In sum, this study reveals that ATXN1 protein family, together with CIC, is critical for development and for regulating key steps in transcriptional control of ECM remodeling. Moreover, these findings raise the interesting possibility about a potential role of these proteins in the pathogenesis of many human diseases associated with defects in ECM remodeling.

Experimental Procedures

Generation of *Atxn1L* knock-out mice

Generation of *Atxn1L* knock-out mice was carried out using a targeting construct previously used to generate a duplication allele (Bowman et al., 2007). To generate a replacement vector, the targeting construct was linearized using SfiI. Identification of targeted cells and generation of chimeras and *Atxn1L*$^{+/-}$ mice were done as previously described (Bowman et al., 2007).

Mouse mating

To test viability of mutant mice at P21 (Table 1), we mated mice using the following combinations: *Atxn1*$^{+/-}$*; Atxn1L*$^{+/-}$ and *Atxn1*$^{+/-}$*; Atxn1L*$^{+/-}$, *Atxn1*$^{+/-}$*; Atxn1L*$^{+/-}$ and *Atxn1*$^{-/-}$*; Atxn1L*$^{+/-}$ or *Atxn1*$^{+/-}$*; Atxn1L*$^{+/-}$ and *Atxn1*$^{+/-}$*; Atxn1L*$^{-/-}$. To investigate the omphalocoele at E18.5-E19 (Table 1), we obtained the embryos from crosses between

Atxn1$^{+/-}$*; Atxn1L*$^{+/-}$ and *Atxn1*$^{+/-}$*; Atxn1L*$^{+/-}$, *Atxn1*$^{+/-}$*; Atxn1L*$^{+/-}$ and *Atxn1*$^{-/-}$*; Atxn1L*$^{+/-}$ or *Atxn1*$^{+/-}$*; Atxn1L*$^{+/-}$ and *Atxn1*$^{+/-}$*; Atxn1L*$^{-/-}$.

Histology

Brain and lung tissues were dissected and fixed with 10% formalin (Sigma) at 4°C overnight. The lungs from mice older than 3 weeks were pressure perfused at 20cm H_2O with 10% formalin at 4°C overnight. Tissues were dehydrated gradually by 70% to 100% EtOH, equilibrated with chloroform overnight, embeded in paraffin blocks, and sectioned at 6 μm thickness. Sections mounted onto slides were stained with H&E for histological analysis. Lungs from more than twenty 2.5-3.5 week old *Atxn1L*$^{-/-}$ and four 2-3 week old *Cic-L*$^{-/-}$ mice were analysed with H&E staining. For Verhoeff staining, ACCUSTAIN Elastic Stain kit (Sigma) was used according to manufacturer's instruction. The step for staining in Van Gieson solution was skipped.

Measurement of the empty space area in E17.5 embryonic lung tissue sections

Four 10x images were captured from H&E-stained lung tissue sections from E17.5 double heterozygous and double null embryos. Each image was converted into 8 bit binary image with ImageJ software. The empty space area was determined by calculating the number of white pixels using ImageJ software and then divided by the number of pixels for whole image area to get the percentage of empty space area in the lung sections.

Immunohistochemistry

The lung tissues embeded in paraffin blocks were sectioned at 6 μm thickness and subjected to the immunohistochemistry using rabbit polyclonal antibodies for CCSP (Abcam, 1:2000) and SFTPC (Millipore, 1:5000). The VECTASTATIN Elite ABC kit (Vector Lab) was used for the immunohistochemistry according to the manufacturer's instruction.

Morphometric analysis

Measurement of mean linear intercept (MLI) was conducted as described previously with some modification (Robbesom et al., 2003). Sixteen 40x images were randomly captured from H&E-stained lung tissue sections from 2.5-3 week old WT, *Atxn1L*$^{-/-}$, and *Atxn1*$^{+/-}$*; Atxn1L*$^{-/-}$ mice and analyzed for the MLI. Total number of counted intercepts was about 900 per each genotype.

Counting the number of alveolar macrophage cells

Bronchoalveolar lavage (BAL) fluid collection and quantitation of airway alveolar macrophage cells were carried out as previously described (Kheradmand et al., 2002). BAL cells were collected by serially instilling and withdrawing 0.7 ml aliquots of PBS from the tracheal cannula. After cells were washed and enumerated, aliquots of 10^5 cells were centrifuged onto glass slides, stained using modified Giemsa, and used to determine the absolute numbers of alveolar macrophage cells.

Determination of the elastin content in the alveolar walls

Measurement of alveolar wall elastin content was conducted as described previously with some modification (Foronjy et al., 2008). Five 40x images were captured from Verhoeff-stained lung tissue sections from 7-9 month old WT and *Atxn1L*$^{-/-}$ mice (n=4 in each genotype). Each 40x image was magnified 4 times to make the stained elastic fibrils easily discernable, and then analyzed for both the whole alveolar wall area and elastic fibrils-occupying area within alveolar walls using ImageJ software. The average elastin percent area for each genotype was calculated as described previously (Foronjy et al., 2008).

Microarray analysis

Hundred ng of lung total RNA from either 6 day-old WT, *Atxn1*$^{-/-}$ or *Atxn1L*$^{-/-}$ mice (3 pairs of WT and *Atxn1*$^{-/-}$ mice and 4 pairs of WT and *Atxn1L*$^{-/-}$ mice) was used for microarray analysis using Affymetrix Mouse Gene 1.0 ST Array. The data were analyzed using Limma package in the Bioconductor R (http://www.bioconductor.org/). The signal intensities were obtained and corrected for background by using Robust Multi-array Analysis (RMA) algorithm (Irizarry et al., 2003). Probes having low signal intensity (< 90) were excluded from the analysis to reduce the inconsistency associated with low-intensity signals. *P* values were calculated with a modified t-test in conjunction with empirical Bayes method (Smyth, 2004). Probes with fold-change > 1.2 and *P* values < 0.05 were considered to be differentially expressed. The GEO accession number of microarray data is GSE29551.

Western blot analysis

Tissues were dissected from mice at either E18.5, P6 or P20 and frozen quickly in liquid nitrogen. In case of lung tissues, the right four lobules were dissected and chopped into several small pieces in cold phosphate buffered saline (PBS) and large blood vessels were removed under dissecting microscope before frozen in liquid nitrogen. The tissues were sonicated in RIPA buffer (150mM NaCl, 50mM Tris-HCl pH 8.0, 2mM EDTA pH 8.0, 1% Triton X-100, 0.5% Deoxychloric acid, 0.1% SDS) with protease and phosphatase inhibitors and incubated on ice for 15 min. After centrifugation at 13,200 rpm for 15 min, the supernatant was taken and 20 μg of that was used for sample preparation. The protein samples were loaded on NuPage 4-20% Bis-Tris gel (Invitrogen) and transferred to Trans-Blot nitrocellulose membrane (Bio-Rad). Primary antibodies for Cic, Atxn1 (11750), and Atxn1L were used as described previously (Bowman et al., 2007). Rabbit polyclonal anti-MMP9 (Abcam) and anti-ETV4 (ProteinTech Group) antibodies were used at 1:1000 and 1:500 dilutions, respectively.

Gelatin zymography

Twenty μg of protein extract from P6 lung or meninge tissues was loaded on Novex 10% Zymogram (Gelatin) gel (Invitrogen). After electrophoresis, developing and staining the gel were carried out according to the manufacturer's manual (Invitrogen).

RNAi

MH-S and A549 cells were cultured in RPMI 1640 media (Invitrogen) supplemented with 10% FBS. They were plated the day before transfection at about 50% confluence in 6cm dishes. The following day, the indicated amount of siRNAs for negative control, Cic, Etv4 (mouse) and ETV4 (human) was transfected using DharmaFECT I transfection reagent (Dharmacon) according to the manufacturer's protocol. Three to four days later, cells were harvested. Protein samples for western blot analysis were prepared by lysis of the cells in cold RIPA buffer for 15 min followed by centrifugation at 1,3000 rpm for 15 min. Total RNA was extracted using Trizol (Invitrogen) and subjected to QRT-PCR analysis. The siRNAs are commercially available (*Cic* siRNA from Dharmacon, mouse *Etv4* stealth siRNAs from Invitrogen and human *ETV4* siRNAs from Ambion). The target sequences of siCic are 5′-GGUGCAACAAGGACCGAAA-3′. The target sequences of siEtv4-1 and siEtv4-2 are 5′-CCUUCUGCAGCAAAUCUCCCGGAAA-3′ and 5′-AGAAGCUCAGGUACCGGACAGUGAU-3′, respectively. The target sequences of siETV4-1 and siETV4-2 are 5′-GGACUUCGCCUACGACUCA-3′ and 5′-CCUGAUUUCCAUUCAGAAA-3′, respectively.

QRT-PCR

Two to three μg of total RNA from lung tissues, MH-S or A549 cells was used for cDNA synthesis using M-MLV-RT (Invitrogen). Quantitative RT-PCR was carried out using commercially available or homemade primers and probes for studied genes. For *Etv1*, 5′-GACCAGCAAGTGCCTTACGT-3′ (Forward), 5′-GACATTTGTTGGTTTCTCGGTACA-3′ (Reverse), and 5′-TCACCAACAGTCAGCGTGGGAGAAA-3′ (Probe) were used. For *Etv4*, 5′-CACTCCCCTACCACCATGGA-3′ (Forward), 5′-GGACTTGATGGCGATTTGTC-3′ (Reverse), and 5′-AGCAGTGCCTTTACTCCAGTGCCTATGA-3′ (Probe) were used. For *Etv5*, 5′-GATTGACAGAAAGAGGAAGTTTGTG-3′ (Forward), 5′-GCAGCTGGCTAAGATCCTGAA-3′ (Reverse), and 5′-CAGATCTGGCTCACGATTCTGAAGAGTTG-3′ (Probe) were used. Taqman Gene Expression Assays (Applied biosystem) were used for detection of *Mmp2* (Mm00439506_m1), *Mmp3* (Mm00440295_m1), *Mmp8* (Mm00772335_m1), *Mmp9* (Mm00442991_m1), *Mmp11* (Mm00485048_m1), *Mmp12* (Mm00500554_m1), *Mmp13* (Mm01168713_m1), *Mmp14* (Mm01318966_m1), *Timp1* (Mm00441818_m1), *Timp2* (Mm00441825_m1) and *Timp3* (Mm00441826_m1). For *Gapdh*, TaqMan Rodent GAPDH control reagent (Applied Biosystem) was used. The SYBR Green was used for detection of PCR amplification of human *ETV4*, *MMP9* and *GAPDH* genes. The primer sequences for *ETV4* are 5′-GCAGTTTGTTCCTGATTTCCA-3′ (Forward) and 5′-ACTCTGGGGCTCCTTCTTG-3′ (Reverse). The primer sequences for *MMP9* are 5′-TCTTCCCTGGAGACCTGAGA-3′ (Forward) and 5′-GAGTGTAACCATAGCGGTACAGG-3′ (Reverse). The primer sequences for *GAPDH* are 5′-AGCCACATCGCTCAGACAC-3′ (Forward) and 5′-GCCCAATACGACCAAATCC-3′ (Reverse).

Chromatin immunoprecipitaion and PCR for mouse Pea3 group gene promoters

Chromatin immunoprecipitation (ChIP) was carried out as previously described (Chahrour et al., 2008) with some modifications. In this experiment, P6 lung tissues and rabbit polyclonal anti-Cic antibody (Abcam) were used. To detect association of Cic with *Etv1*, *Etv4* and *Etv5* promoters, the following primers were used for PCR. For *Etv1* promoter, 5′-GAGGAACTTGGGCCTTTGTTATG-3′ (Forward) and 5′-TGCTTTCGAGCAGGGGGC-3′ (Reverse) were used for PCR. For *Etv4* promoter, 5′-CGTGGAGAAGCTGCCGGGTC-3′ (Forward) and 5′-CTCCCCACCGGTTCCCTTTG-3′ (Reverse) were used for PCR. For *Etv5* promoter, 5′-GGTGCAGGCCGAGGCCAGGG-3′ (Forward) and 5′-CATTGACCAATCAGCACCGG-3′ (Reverse) were used for PCR.

Statistical analyses

For statistical analysis, all experiments were carried out more than three times independently. The Western blots were quantified using ImageJ software package. Statistical significance between control values and experimental values was determined using Student's *t* test (two-tailed, two-sample unequal variance). Statistical significance is represented with asterisks.

Supplementary Material

Refer to Web version on PubMed Central for supplementary material.

Acknowledgments

We thank Dr. Moghaddam for helping us with inflated fixation of lung tissues and Jounghwa Won for the morphometric analysis. We are grateful to members of the Zoghbi laboratory for helpful discussions and comments

on the manuscript. The morphological studies were performed in the Molecular Morphology Core Laboratory of the NIDDK-sponsored Texas Medical Center Digestive Disease Center, DK 56338. This research was supported by NIH grants NS27699 and HD24064 to H.Y.Z. H.Y.Z. is an investigator with the Howard Hughes Medical Institute.

Reference

Ajuria L, Nieva C, Winkler C, Kuo D, Samper N, Andreu MJ, Helman A, González-Crespo S, Paroush Z, Courey AJ, et al. Capicua DNA-binding sites are general response elements for RTK signaling in Drosophila. Development. 2011; 138:915–924. [PubMed: 21270056]

Antoniou SA, Antoniou GA, Granderath FA, Simopoulos C. The role of matrix metalloproteinases in the pathogenesis of abdominal wall hernias. Eur. J. Clin. Invest. 2009; 39:953–959. [PubMed: 19656168]

Banfi S, Servadio A, Chung MY, Kwiatkowski TJ, McCall AE, Duvick LA, Shen Y, Roth EJ, Orr HT, Zoghbi HY. Identification and characterization of the gene causing type 1 spinocerebellar ataxia. Nat. Genet. 1994; 7:513–520. [PubMed: 7951322]

Bettegowda C, Agrawal N, Jiao Y, Sausen M, Wood LD, Hruban RH, Rodriguez FJ, Cahill DP, McLendon R, Riggins G, et al. Mutations in CIC and FUBP1 Contribute to Human Oligodendroglioma. Science. 2011 Available at: http://www.ncbi.nlm.nih.gov/pubmed/21817013.

Bowman AB, Lam YC, Jafar-Nejad P, Chen H-K, Richman R, Samaco RC, Fryer JD, Kahle JJ, Orr HT, Zoghbi HY. Duplication of Atxn1l suppresses SCA1 neuropathology by decreasing incorporation of polyglutamine-expanded ataxin-1 into native complexes. Nat. Genet. 2007; 39:373–379. [PubMed: 17322884]

Chahrour M, Jung SY, Shaw C, Zhou X, Wong STC, Qin J, Zoghbi HY. MeCP2, a key contributor to neurological disease, activates and represses transcription. Science. 2008; 320:1224–1229. [PubMed: 18511691]

Crespo-Barreto J, Fryer JD, Shaw CA, Orr HT, Zoghbi HY. Partial loss of ataxin-1 function contributes to transcriptional dysregulation in spinocerebellar ataxia type 1 pathogenesis. PLoS Genet. 2010; 6:e1001021. [PubMed: 20628574]

Dennis G, Sherman BT, Hosack DA, Yang J, Gao W, Lane HC, Lempicki RA. DAVID: Database for Annotation, Visualization, and Integrated Discovery. Genome Biol. 2003; 4:P3. [PubMed: 12734009]

Díaz-Sanjuán T, García-Ruiz I, Rodríguez-Juan C, Muñoz-Yagüe T, Solís-Muñoz P, Solís-Herruzo JA. Interferon alpha increases metalloproteinase-13 gene expression through a polyomavirus enhancer activator 3-dependent pathway in hepatic stellate cells. J. Hepatol. 2009; 50:128–139. [PubMed: 19014879]

Dissanayake K, Toth R, Blakey J, Olsson O, Campbell DG, Prescott AR, MacKintosh C. ERK/p90(RSK)/14-3-3 signalling has an impact on expression of PEA3 Ets transcription factors via the transcriptional repressor capicúa. Biochem. J. 2011; 433:515–525. [PubMed: 21087211]

Finlay GA, Russell KJ, McMahon KJ, D'arcy EM, Masterson JB, FitzGerald MX, O'Connor CM. Elevated levels of matrix metalloproteinases in bronchoalveolar lavage fluid of emphysematous patients. Thorax. 1997; 52:502–506. [PubMed: 9227714]

Foronjy RF, Okada Y, Cole R, D'Armiento J. Progressive adult-onset emphysema in transgenic mice expressing human MMP-1 in the lung. Am. J. Physiol. Lung Cell Mol. Physiol. 2003; 284:L727–737. [PubMed: 12676763]

Foronjy R, Nkyimbeng T, Wallace A, Thankachen J, Okada Y, Lemaitre V, D'Armiento J. Transgenic expression of matrix metalloproteinase-9 causes adult-onset emphysema in mice associated with the loss of alveolar elastin. Am. J. Physiol. Lung Cell Mol. Physiol. 2008; 294:L1149–1157. [PubMed: 18408070]

Greenlee KJ, Werb Z, Kheradmand F. Matrix metalloproteinases in lung: multiple, multifarious, and multifaceted. Physiol. Rev. 2007; 87:69–98. [PubMed: 17237343]

Gum R, Lengyel E, Juarez J, Chen JH, Sato H, Seiki M, Boyd D. Stimulation of 92-kDa gelatinase B promoter activity by ras is mitogen-activated protein kinase kinase 1-independent and requires multiple transcription factor binding sites including closely spaced PEA3/ets and AP-1 sequences. J. Biol. Chem. 1996; 271:10672–10680. [PubMed: 8631874]

Hida K, Shindoh M, Yasuda M, Hanzawa M, Funaoka K, Kohgo T, Amemiya A, Totsuka Y, Yoshida K, Fujinaga K. Antisense E1AF transfection restrains oral cancer invasion by reducing matrix metalloproteinase activities. Am. J. Pathol. 1997; 150:2125–2132. [PubMed: 9176403]

Irizarry RA, Hobbs B, Collin F, Beazer-Barclay YD, Antonellis KJ, Scherf U, Speed TP. Exploration, normalization, and summaries of high density oligonucleotide array probe level data. Biostatistics. 2003; 4:249–264. [PubMed: 12925520]

Jiménez G, Guichet A, Ephrussi A, Casanova J. Relief of gene repression by torso RTK signaling: role of capicua in Drosophila terminal and dorsoventral patterning. Genes Dev. 2000; 14:224–231. [PubMed: 10652276]

Kan Z, Jaiswal BS, Stinson J, Janakiraman V, Bhatt D, Stern HM, Yue P, Haverty PM, Bourgon R, Zheng J, et al. Diverse somatic mutation patterns and pathway alterations in human cancers. Nature. 2010; 466:869–873. [PubMed: 20668451]

Kawamura-Saito M, Yamazaki Y, Kaneko K, Kawaguchi N, Kanda H, Mukai H, Gotoh T, Motoi T, Fukayama M, Aburatani H, et al. Fusion between CIC and DUX4 up-regulates PEA3 family genes in Ewing-like sarcomas with t(4;19)(q35;q13) translocation. Hum. Mol. Genet. 2006; 15:2125–2137. [PubMed: 16717057]

Kessenbrock K, Plaks V, Werb Z. Matrix metalloproteinases: regulators of the tumor microenvironment. Cell. 2010; 141:52–67. [PubMed: 20371345]

Kheradmand F, Kiss A, Xu J, Lee S-H, Kolattukudy PE, Corry DB. A protease-activated pathway underlying Th cell type 2 activation and allergic lung disease. J. Immunol. 2002; 169:5904–5911. [PubMed: 12421974]

Kurpios NA, Sabolic NA, Shepherd TG, Fidalgo GM, Hassell JA. Function of PEA3 Ets transcription factors in mammary gland development and oncogenesis. J Mammary Gland Biol Neoplasia. 2003; 8:177–190. [PubMed: 14635793]

Lam YC, Bowman AB, Jafar-Nejad P, Lim J, Richman R, Fryer JD, Hyun ED, Duvick LA, Orr HT, Botas J, et al. ATAXIN-1 interacts with the repressor Capicua in its native complex to cause SCA1 neuropathology. Cell. 2006; 127:1335–1347. [PubMed: 17190598]

Leco KJ, Waterhouse P, Sanchez OH, Gowing KL, Poole AR, Wakeham A, Mak TW, Khokha R. Spontaneous air space enlargement in the lungs of mice lacking tissue inhibitor of metalloproteinases-3 (TIMP-3). J. Clin. Invest. 2001; 108:817–829. [PubMed: 11560951]

Lim J, Hao T, Shaw C, Patel AJ, Szabó G, Rual J-F, Fisk CJ, Li N, Smolyar A, Hill DE, et al. A protein-protein interaction network for human inherited ataxias and disorders of Purkinje cell degeneration. Cell. 2006; 125:801–814. [PubMed: 16713569]

Liu Y, Jiang H, Crawford HC, Hogan BLM. Role for ETS domain transcription factors Pea3/Erm in mouse lung development. Dev. Biol. 2003; 261:10–24. [PubMed: 12941618]

Matilla A, Roberson ED, Banfi S, Morales J, Armstrong DL, Burright EN, Orr HT, Sweatt JD, Zoghbi HY, Matzuk MM. Mice lacking ataxin-1 display learning deficits and decreased hippocampal paired-pulse facilitation. J. Neurosci. 1998; 18:5508–5516. [PubMed: 9651231]

Mizutani A, Wang L, Rajan H, Vig PJS, Alaynick WA, Thaler JP, Tsai C-C. Boat, an AXH domain protein, suppresses the cytotoxicity of mutant ataxin-1. EMBO J. 2005; 24:3339–3351. [PubMed: 16121196]

Muñoz NM, Upton M, Rojas A, Washington MK, Lin L, Chytil A, Sozmen EG, Madison BB, Pozzi A, Moon RT, et al. Transforming growth factor beta receptor type II inactivation induces the malignant transformation of intestinal neoplasms initiated by Apc mutation. Cancer Res. 2006; 66:9837–9844. [PubMed: 17047044]

Oblander SA, Zhou Z, Gálvez BG, Starcher B, Shannon JM, Durbeej M, Arroyo AG, Tryggvason K, Apte SS. Distinctive functions of membrane type 1 matrix-metalloprotease (MT1-MMP or MMP-14) in lung and submandibular gland development are independent of its role in pro-MMP-2 activation. Dev. Biol. 2005; 277:255–269. [PubMed: 15572153]

Orr HT, Chung MY, Banfi S, Kwiatkowski TJ, Servadio A, Beaudet AL, McCall AE, Duvick LA, Ranum LP, Zoghbi HY. Expansion of an unstable trinucleotide CAG repeat in spinocerebellar ataxia type 1. Nat. Genet. 1993; 4:221–226. [PubMed: 8358429]

Oshima M, Oshima H, Taketo MM. TGF-beta receptor type II deficiency results in defects of yolk sac hematopoiesis and vasculogenesis. Dev. Biol. 1996; 179:297–302. [PubMed: 8873772]

Qin L, Liao L, Redmond A, Young L, Yuan Y, Chen H, O'Malley BW, Xu J. The AIB1 oncogene promotes breast cancer metastasis by activation of PEA3-mediated matrix metalloproteinase 2 (MMP2) and MMP9 expression. Mol. Cell. Biol. 2008; 28:5937–5950. [PubMed: 18644862]

Qu P, Du H, Wang X, Yan C. Matrix metalloproteinase 12 overexpression in lung epithelial cells plays a key role in emphysema to lung bronchioalveolar adenocarcinoma transition. Cancer Res. 2009; 69:7252–7261. [PubMed: 19706765]

Robbesom AA, Versteeg EMM, Veerkamp JH, van Krieken JHJM, Bulten HJ, Smits HTJ, Willems LNA, van Herwaarden CLA, Dekhuijzen PNR, van Kuppevelt TH. Morphological quantification of emphysema in small human lung specimens: comparison of methods and relation with clinical data. Mod. Pathol. 2003; 16:1–7. [PubMed: 12527706]

Roch F, Jiménez G, Casanova J. EGFR signalling inhibits Capicua-dependent repression during specification of Drosophila wing veins. Development. 2002; 129:993–1002. [PubMed: 11861482]

Roy R, Yang J, Moses MA. Matrix metalloproteinases as novel biomarkers and potential therapeutic targets in human cancer. J. Clin. Oncol. 2009; 27:5287–5297. [PubMed: 19738110]

Shi W, Bellusci S, Warburton D. Lung development and adult lung diseases. Chest. 2007; 132:651–656. [PubMed: 17699136]

Siepel A, Bejerano G, Pedersen JS, Hinrichs AS, Hou M, Rosenbloom K, Clawson H, Spieth J, Hillier LW, Richards S, et al. Evolutionarily conserved elements in vertebrate, insect, worm, and yeast genomes. Genome Res. 2005; 15:1034–1050. [PubMed: 16024819]

Sjöblom T, Jones S, Wood LD, Parsons DW, Lin J, Barber TD, Mandelker D, Leary RJ, Ptak J, Silliman N, et al. The consensus coding sequences of human breast and colorectal cancers. Science. 2006; 314:268–274. [PubMed: 16959974]

Smyth GK. Linear models and empirical bayes methods for assessing differential expression in microarray experiments. Stat Appl Genet Mol Biol. 2004; 3 Article 3.

Suzuki N, Labosky PA, Furuta Y, Hargett L, Dunn R, Fogo AB, Takahara K, Peters DM, Greenspan DS, Hogan BL. Failure of ventral body wall closure in mouse embryos lacking a procollagen C-proteinase encoded by Bmp1, a mammalian gene related to Drosophila tolloid. Development. 1996; 122:3587–3595. [PubMed: 8951074]

Thumkeo D, Shimizu Y, Sakamoto S, Yamada S, Narumiya S. ROCK-I and ROCK-II cooperatively regulate closure of eyelid and ventral body wall in mouse embryo. Genes Cells. 2005; 10:825–834. [PubMed: 16098146]

Wyss-Coray T, Feng L, Masliah E, Ruppe MD, Lee HS, Toggas SM, Rockenstein EM, Mucke L. Increased central nervous system production of extracellular matrix components and development of hydrocephalus in transgenic mice overexpressing transforming growth factor-beta 1. Am. J. Pathol. 1995; 147:53–67. [PubMed: 7604885]

Yan C, Boyd DD. Regulation of matrix metalloproteinase gene expression. J. Cell. Physiol. 2007; 211:19–26. [PubMed: 17167774]

Zechel J, Gohil H, Lust WD, Cohen A. Alterations in matrix metalloproteinase-9 levels and tissue inhibitor of matrix metalloproteinases-1 expression in a transforming growth factor-beta transgenic model of hydrocephalus. J. Neurosci. Res. 2002; 69:662–668. [PubMed: 12210832]

Zhao K, Sun H, Shan Y, Mao BY, Zhang H. Cerebrospinal fluid absorption disorder of arachnoid villi in a canine model of hydrocephalus. Neurol India. 2010; 58:371–376. [PubMed: 20644263]

Zoghbi HY, Orr HT. Spinocerebellar ataxia type 1. Semin. Cell Biol. 1995; 6:29–35. [PubMed: 7620119]

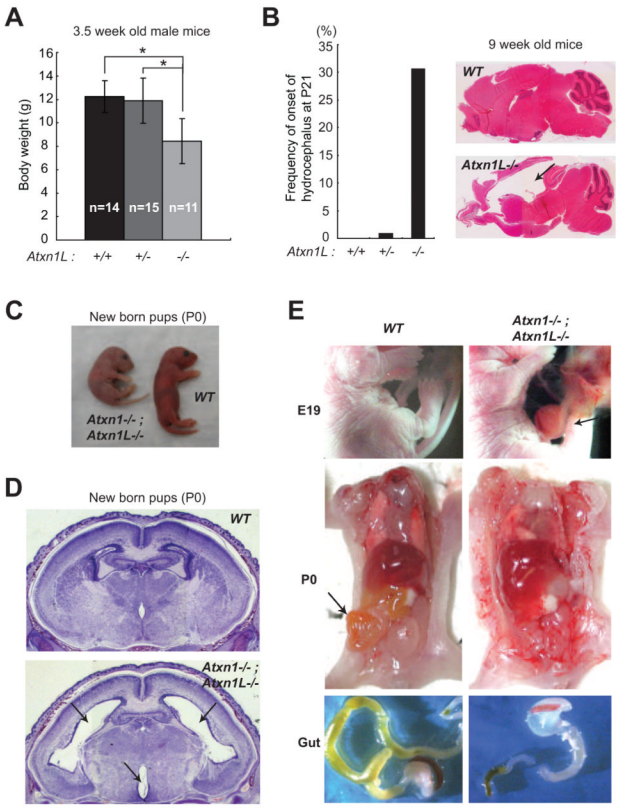

Figure 1.

Developmental abnormalities in *Atxn1* and *Atxn1L* double mutant mice.

(A) Bar graph representation of the average body weight of *Atxn1L*$^{-/-}$ and littermates at 3.5 weeks after birth. *P<0.05. Error bars show s.d.

(B) Incidence of hydrocephalus in *Atxn1L*$^{-/-}$ mutants after weaning age. Right panel shows hematoxylin and eosin (H&E) staining of formalin-fixed section of whole brains from hydrocephalic *Atxn1L*-null mouse and WT littermate at 9 weeks after birth.

(C) Picture of *Atxn1*$^{-/-}$*; Atxn1L*$^{-/-}$ and wild type neonates.

(D) Hydrocephalus in *Atxn1*$^{-/-}$*; Atxn1L*$^{-/-}$ mice. H&E staining of formalin-fixed section of whole brains from hydrocephalic *Atxn1*$^{-/-}$*; Atxn1L*$^{-/-}$ and WT littermate at P0.

(E) Abdominal wall closure defect in *Atxn1*$^{-/-}$*; Atxn1L*$^{-/-}$ mice. Upper pannel: images showing the abdominal wall closure defect in the *Atxn1*$^{-/-}$*; Atxn1L*$^{-/-}$ at E19. The arrow indicates protruding gut into the umbilical ring (omphalocoele). Middle panel: Abdominal anatomy on WT and *Atxn1*$^{-/-}$*; Atxn1L*$^{-/-}$ neonates. Arrow indicates the midgut. Lower panel shows the remaining guts dissected from WT and the *Atxn1*$^{-/-}$*; Atxn1L*$^{-/-}$ neonates.

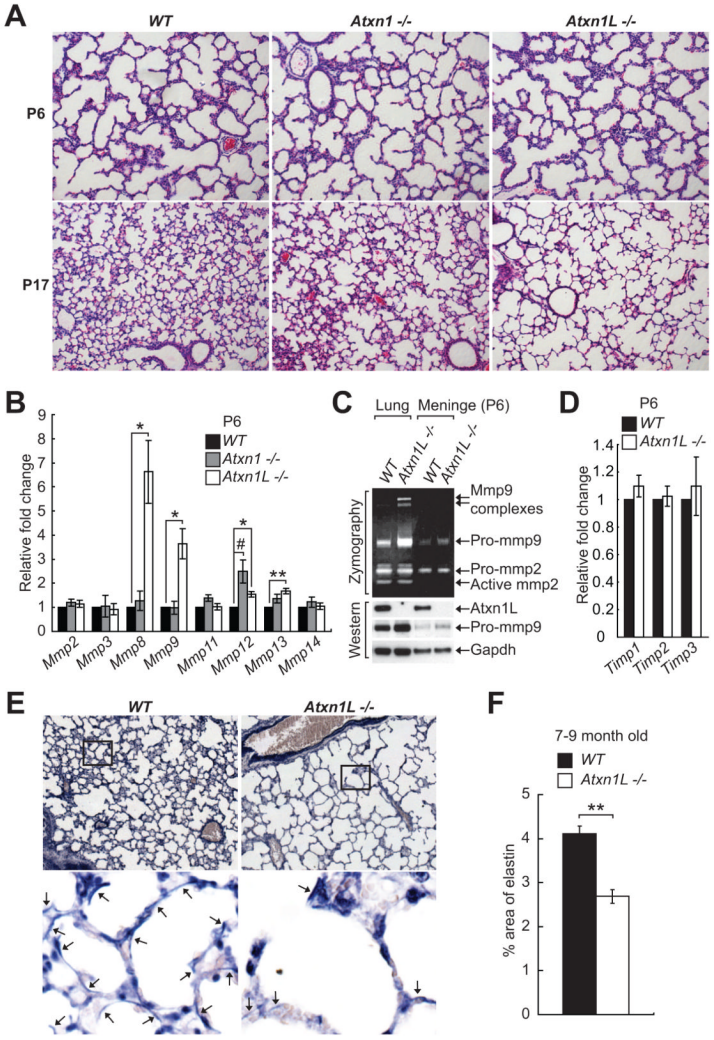

Figure 2.

Alveolarization defects in *Atxn1L*$^{-/-}$ mice.

(A) H&E staining of formalin-fixed section of lung tissues from WT, *Atxn1*$^{-/-}$ and *Atxn1L*$^{-/-}$ at either P6 or P17. The alveolarization defect causing enlargement of the air spaces is observed in *Atxn1L*$^{-/-}$ mice at P17.

(B) QRT-PCR analysis of levels of eight *Mmp* genes using total RNA from the lungs of either WT, *Atxn1*$^{-/-}$ or *Atxn1L*$^{-/-}$ at P6 (n=4 per each genotype). *P<0.05. #P=0.0542. All error bars show s.e.m.

(C) Gelatin zymography and Western blot analysis showing increased Mmp9 levels in lung and meningial tissues from 6 day-old *Atxn1L*$^{-/-}$ mice. Twenty μg of lung extract and 10 μg of meningial tissue extract were loaded in each lane.

(D) QRT-PCR analysis for *Timp1, Timp2* and *Timp3* levels in the lungs from 6 day-old wild-type and *Atxn1L*$^{-/-}$ mice (n=3 per each genotype).

(E) Verhoeff staining for elastin of alveolar walls. Formalin-fixed section of lung tissues from 7-9 month-old WT and *Atxn1L*$^{-/-}$ mice was used. Marked decrease in elastic fiber formation on alveolar walls is found in *Atxn1L*$^{-/-}$ mice with the alveolarization defects, compared with WT. The upper pictures show 10X magnified images for Verhoeff staining. The lower pictures represent enlarged images (80X) for the boxed areas in the upper pictures. Arrows indicate elastic fibers.

(F) Bar graph for quantification of percentage of elastic fibril positive area within alveolar walls (n=4 per each genotype). *P<0.05. All error bars show s.e.m.

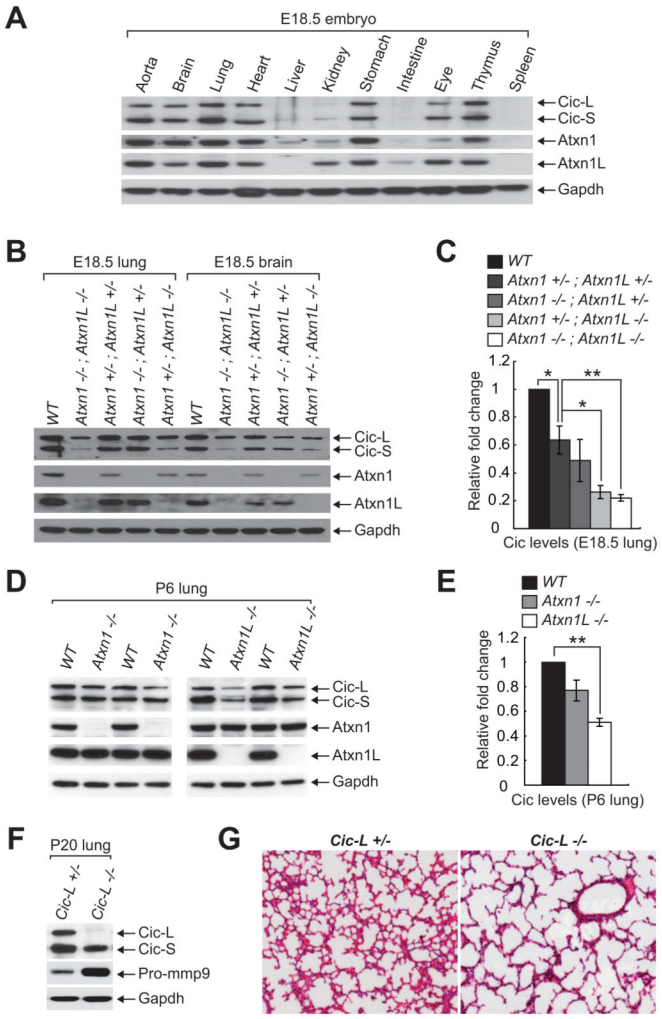

Figure 3.

Loss of Atxn1/Atxn1L-Cic complexes causes the alveolarization defects.

(A) Western blot analysis for Atxn1, Atxn1L and Cic using several different tissues from E18.5 wild-type embryos. Twenty μg of protein was loaded in each lane.

(B) Representative Western blot image showing the Cic levels in lung and brain tissues from each genotype at E18.5**.**

(C) Quantitative analysis of the Cic levels in the lung from each genotype at E18.5 (n=3 per each genotype). *P<0.05. All error bars show s.e.m.

(D) Representative Western blot image showing the Cic levels in lung tissues from each genotype at P6.

(E) Quantitative analysis of the Cic levels in the lung tissues from each genotype at P6 (n=3 per each genotype). **P<0.01. All error bars show s.e.m.

(F) Western blot image showing increased Mmp9 levels in lung tissues from *Cic-L*$^{-/-}$ compared with *Cic-L*$^{+/-}$ mice.

(G) H&E staining of formalin-fixed lung tissues from the *Cic-L*$^{-/-}$ and *Cic-L*$^{+/-}$ mice at P20. Severe alveolarization defects are observed in *Cic-L*$^{-/-}$ mice.

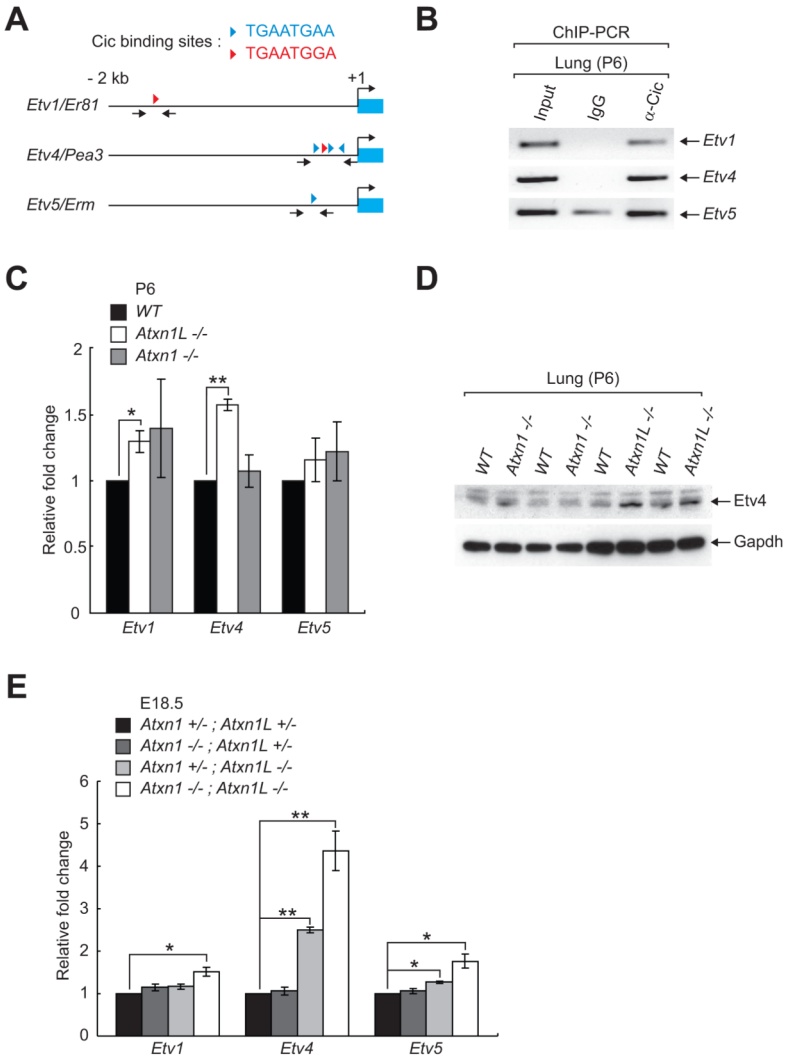

Figure 4.

Derepression of *Pea3* group genes by the loss of Atxn1 and Atxn1L.

(A) Schematic diagram for the location of Cic binding sites (Blue arrow head: TGAATGAA, Red arrow head: TGAATGGA) in *Pea3* group gene promoter regions. Black arrows indicate primers designed to amplify *Pea3* group gene promoter regions containing Cic binding sites by PCR. Transcription start site (+1) of each gene was determined based on the following NCBI reference sequences (NM_007960.4 for *Etv1*, NM_008815.2 for *Etv4* and NM_023794.2 for *Etv5*).

(B) ChIP-PCR analysis showing Cic promoter occupancy of *Pea3* group genes in P6 lung tissue.

(C) QRT-PCR analysis of *Etv1*, *Etv4* and *Etv5* expression levels using total RNA from the lungs of WT, *Atxn1*$^{-/-}$ and *Atxn1L*$^{-/-}$ mice (P6, n=4 per each genotype). *P<0.05. All error bars show s.e.m.

(D) Western blot image showing an increase in Etv4 protein levels in lung tissues from *Atxn1L*$^{-/-}$ mice. In contrast, Etv4 protein levels are normal in *Atxn1*$^{-/-}$ mice.

(E) QRT-PCR analysis of levels of *Etv1*, *Etv4* and *Etv5* using total RNA from the lungs of embryos of each genotype (E18.5, n=4 per each genotype). *P<0.05 and **P<0.01. All error bars show s.e.m.

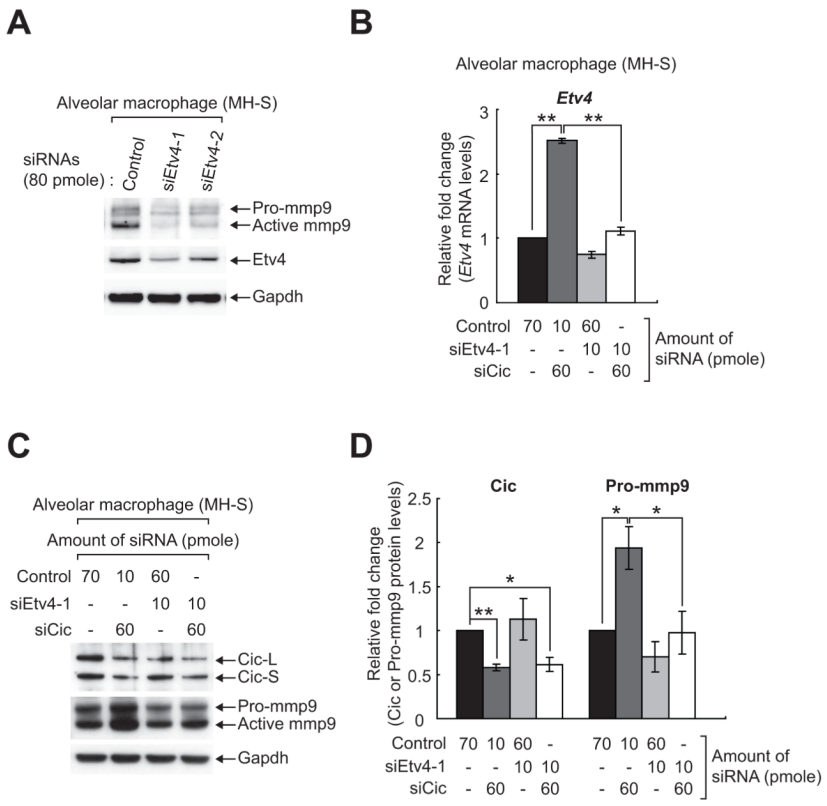

Figure 5.

Derepression of *Etv4* up-regulates Mmp9 levels in alveolar macrophage cells.

(A) Western blot image showing a decrease in Mmp9 levels upon knock-down of *Etv4* in MH-S cells.

(B) QRT-PCR analysis for changes in *Etv4* levels upon treatment of MH-S cells with four different combinations of siRNAs (negative control, *Cic* and *Etv4*). Three independent experiments were carried out. *P<0.05 and **P<0.01. All error bars show s.e.m.

(C) Representative Western blot image for changes in Mmp9 and Cic levels upon treatment of MH-S cells with four different combinations of siRNAs (negative control, *Cic* and *Etv4*).

(D) Quantitative analysis of Cic and Mmp9 levels based on Western blot images from **(C)**. Three independent experiments were carried out. *P<0.05 and **P<0.01. All error bars show s.e.m.

Table 1

Viability and incidence for gut loss (at P0) and omphalocoele (at E18.5-E19) per each genotype

Genotype	Observed (Expected [a]) at P21 on mixed background	Observed (Expected) at P0 on C57BL/6 background	Omphalocoele at E18.5-E19	Gut loss at P0
Atxn1 +/+ ; *Atxn1L* +/+	8 (8)	15 (11.125)	0/5	0/15
Atxn1 +/− ; *Atxn1L* +/+	20 (23)	21 (22.25)	0/5	0/21
Atxn1 −/− ; *Atxn1L* +/+	28 (19)	17 (11.125)	0/10	0/17
Atxn1 +/+ ; *Atxn1L* +/−	12 (14)	21 (22.25)	0/10	0/21
Atxn1 +/+ ; *Atxn1L* −/−	5 (5)	18 (11.125)	0/6	1/18
Atxn1 +/− ; *Atxn1L* +/−	54 (41)	39 (44.5)	0/31	0/39
Atxn1 −/− ; *Atxn1L* +/−	41 (35)	17 (22.25)	0/9	2/17
Atxn1 +/− ; *Atxn1L* −/−	11 (19)	19 (22.25)	2/11	3/19
Atxn1 −/− ; *Atxn1L* −/−	0 (15)	11 (11.125)	5/11	5/11
Total	179	178	7/98	11/178

[a] The number of animals expected to be observed based on Mendelian genetics.

Table 2

Incidence for the onset of three phenotypes (hydrocephalus, omphalocoele and lung alveolarization defect) in WT, *Atxn1*$^{-/-}$, *Atxn1L*$^{-/-}$, *Atxn1*$^{+/-}$; *Atxn1L*$^{-/-}$ and *Atxn1*$^{-/-}$; *Atxn1L*$^{-/-}$ mice

Genotype	Hydrocephalus (at P0)	Omphalocoele (at E18.5-P0)	Lung alveolarization defect (at P17-P23)
Atxn1 +/+ ; *Atxn1L* +/+	0% (0/8)	0% (0/20)	0% (0/33)
Atxn1 −/− ; *Atxn1L* +/+	0% (0/10)	0% (0/27)	0% (0/13)
Atxn1 +/+ ; *Atxn1L* −/−	11% (1/9)	4% (1/24)	65% (13/20)
Atxn1 +/− ; *Atxn1L* −/−	30% (3/10)	17% (5/30)	100% (2/2)[a]
Atxn1 −/− ; *Atxn1L* −/−	75% (3/4)	45% (10/22)	N.D.[b]

[a] A majority of *Atxn1*$^{+/-}$; *Atxn1L*$^{-/-}$ mice died before weaning age (P21) on C57BL/6J background. Only two survivors were subjected to the analysis for the lung alveolarization.

[b] Not Determined.